Two-photon spectroscopy of samarium(III) in the elpasolite $Cs_2NaYCl_6:Sm^{3+}$

1999 J. Phys.: Condens. Matter 11 7867

(http://iopscience.iop.org/0953-8984/11/40/312)

J. Phys.: Condens. Matter **11** (1999) 7867–7879. Printed in the UK PII: S0953-8984(99)05481-8

Two-photon spectroscopy of samarium(III) in the elpasolite Cs_2NaYCl_6:Sm^{3+}

J R G Thorne†, A Karunathilake†, Han Choi†, R G Denning† and T Luxbacher‡

† Department of Chemistry, University of Oxford, Inorganic Chemistry Laboratory, South Parks Road, Oxford, OX1 3QR, UK
‡ Graz Technical University Institut fur Physikalische und Theoretische Chemie, Rechbauerstrasse 12, A-8010 Graz, Austria

Received 24 June 1999

Abstract. We present polarized two-photon excitation (TPE) spectra for samarium(III) f^5 in the elpasolite Cs_2NaYCl_6. Approximately 80 levels have been assigned up to 29 000 cm^{-1} with the aid of a one-electron crystal field Hamiltonian, representing the most complete and extensive data set so far reported for Sm(III) at a cubic site. Deviations from the predictions of one-electron theory are discussed in terms of the spin correlated crystal field (SCCF).

1. Introduction

The levels of samarium(III) in an octahedral crystal field have been previously studied in $Cs_2NaSmCl_6$ [1] and in Cs_2NaYCl_6 doped with samarium [2–4] by absorption and emission spectroscopy. Using the same free ion and crystal field Hamiltonian as in this work, 28 levels belonging principally to the low lying ^6H and ^6F multiplets of Sm^{3+} have been identified [5].

An energy level diagram, in the absence of the crystal field perturbation, for samarium(III) is shown in figure 1. It is intended to serve as a guide to the excited state manifold in the subsequent discussion. One-photon and two-photon absorption are followed by non-radiative decay to the ^4G manifold from which emission occurs to the ^6H_J crystal field levels.

In this paper, which is part of a series [6–12] covering the two-photon excitation spectroscopy of Cs_2NaLnX_6 elpasolites, we use a one-electron crystal-field Hamiltonian to determine the energies and symmetries of a much larger sequence of levels in Cs_2NaYCl_6:Sm^{3+} than has previously been identified. We report many of our observations, for example those relating to polarization selection rules and transition intensities, in comparison to the studied systems $Cs_2NaTbCl_6$ [6–11] and $Cs_2NaEuCl_6$ [12].

2. Experiment

Crystals of $Cs_2NaY_{1-x}Sm_xCl_6$ were grown by the Bridgman technique [13], oriented by Laue back reflection, and cut and polished with faces perpendicular to {100}. Low temperature emission spectra, for comparison with published work, were recorded excited at 355 nm.

0953-8984/99/407867+13$30.00

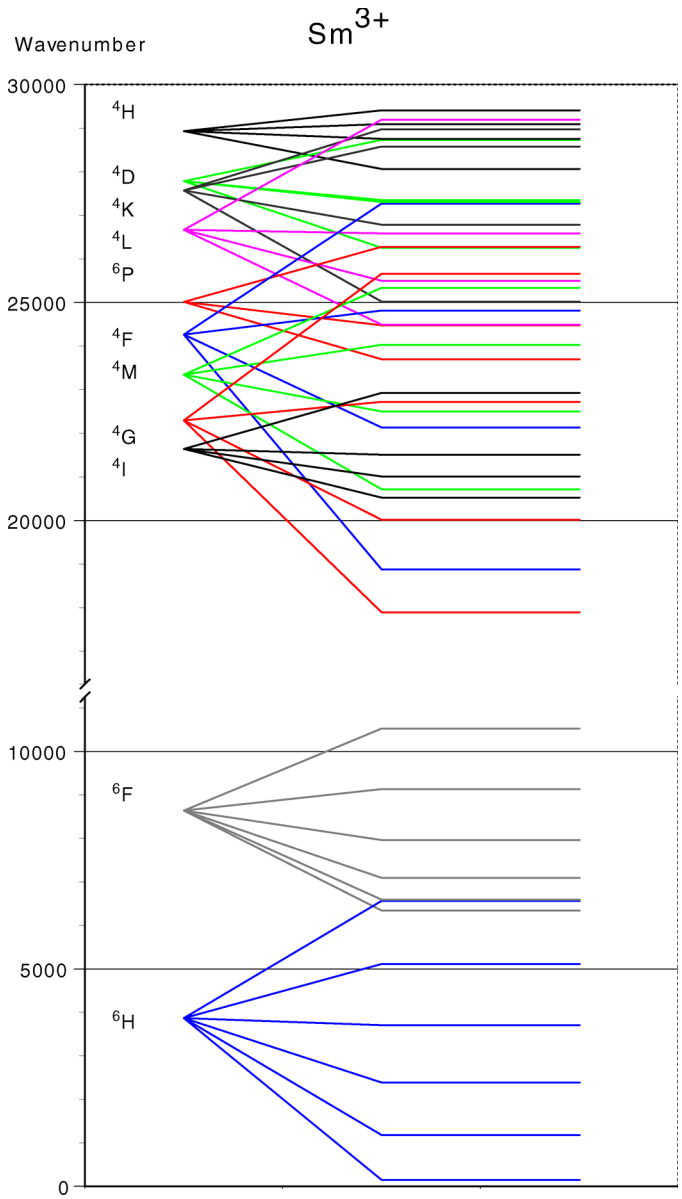

Figure 1. Energy level diagram for samarium(III) in zero field, illustrating the effects of spin–orbit coupling. The levels were calculated using the free ion parameters for $Cs_2NaSm_{0.5}Y_{0.5}Cl_6$ in table 2. (SL) energies are determined from the Russell–Saunders (SLJ) barycentres.

There is evidence that neat $Cs_2NaSmCl_6$ undergoes a phase transition below $\sim$ 100 K to a non-cubic phase [14]. Doped in the Cs_2NaYCl_6 lattice, the $SmCl_6^{3-}$ moiety is not subject to this distortion.

TPE spectra were recorded by monitoring the emission intensity near 570 nm (17 500 cm^{-1}) as a function of the excitation energy from a Nd:YAG pumped Spectra Physics PDL3 dye laser. Optical frequencies in the range 17 700–18 900 cm^{-1} were generated by second Stokes Raman shifting.

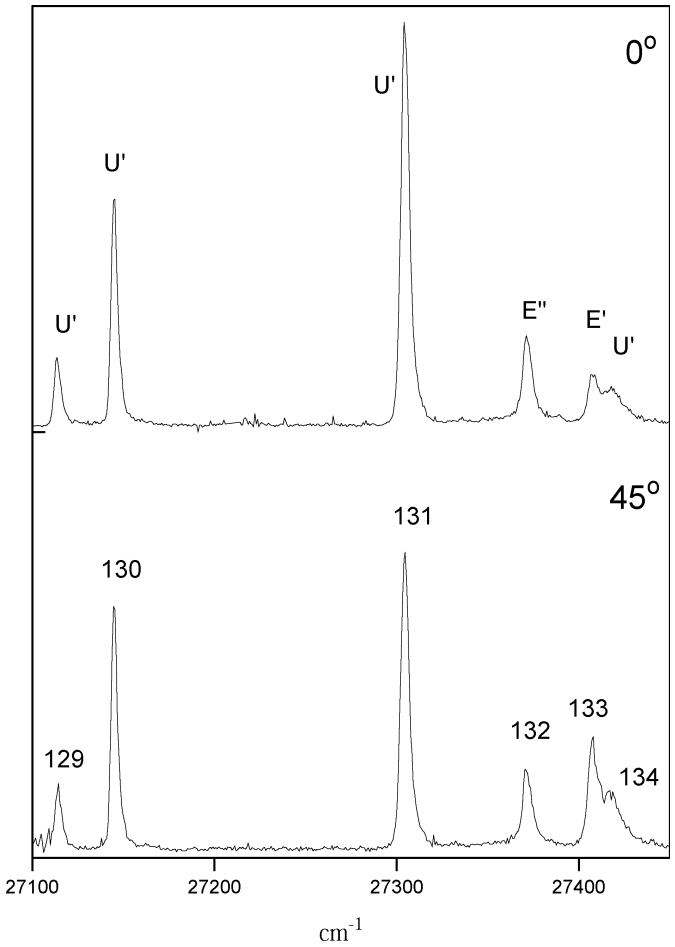

Figure 2. Detail from two-photon spectrum of $Cs_2NaSm_{0.5}Y_{0.5}Cl_6$ at 10 K, illustrating polarization dependent selection rules.

The samarium (III) ion has a window of linear absorption transparency between 11 000 and 17 000 cm^{-1}, potentially allowing non-resonant two-photon excitation (TPE) to states up to nearly 34 000 cm^{-1}. In practice, two-photon excitation was detectable between 9000 cm^{-1} and 14 500 cm^{-1}. The low lying single-photon transitions to ^6F do not obscure two photon transitions. In practice, the proximity of fluorescence to the single-photon excitation frequency set an upper limit for two-photon state detection near 29 000 cm^{-1}.

The samarium(III) ion is not quite such a good candidate for a comprehensive two-photon study as europium(III) and terbium(III), principally due to the shortened fluorescence lifetime and associated low quantum yield, associated with cross relaxation processes [13]. Spectra were recorded at 70 K and 10 K. Those presented in figure 3 are for $Cs_2NaY_{0.5}Sm_{0.5}Cl_6$ at 70 K and represent the more complete polarized data set. Line positions (vacuum wavenumbers) quoted in table 1 are at 10 K, although the spectral shifts from 70 K are less than 2 cm^{-1}. The observed emission decayed with a lifetime of $\sim$ 100 μs at low temperature. We estimate the number of photons detected experimentally to be approximately two orders of magnitude less than for Tb(III) and Eu(III) with consequent increase of signal to noise ratio.

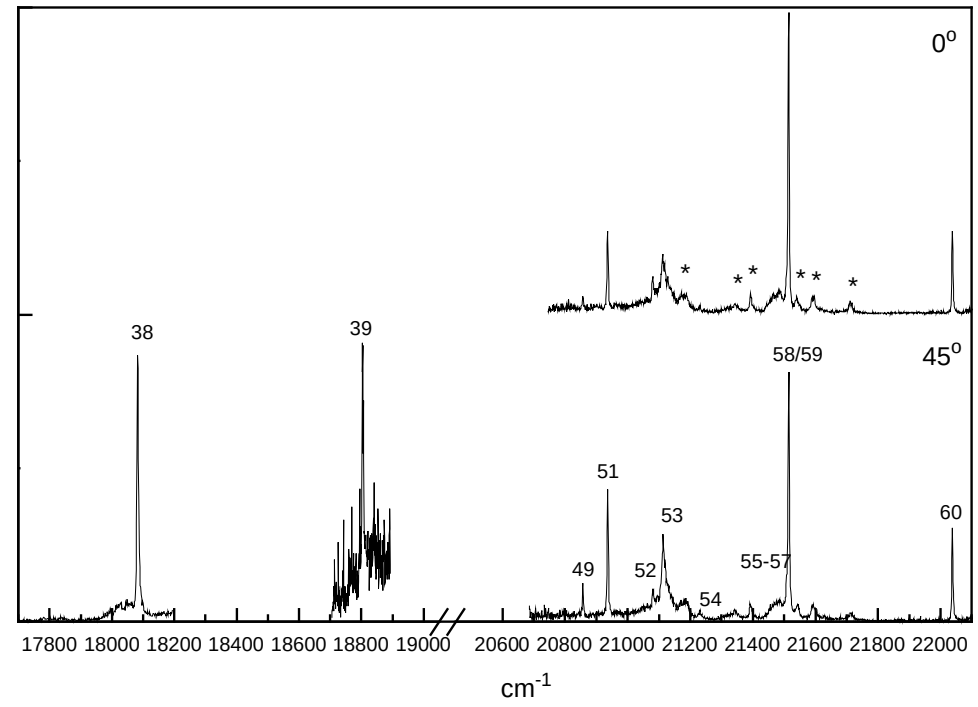

(a)

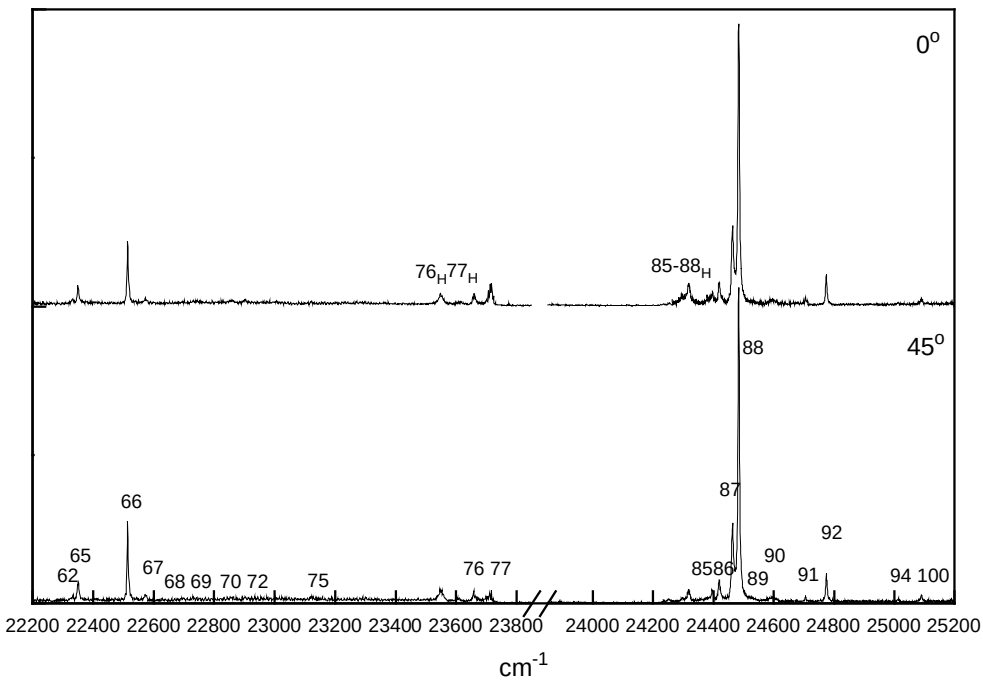

(b)

Figure 3. TPE spectra for $Cs_2NaSm_{0.5}Y_{0.5}Cl_6$ at 70 K, for polarizations with $\alpha = 0^\circ$ and $\alpha = 45^\circ$. Numbers indicate the final state level sequence in table 1. H = hot band; * = Excited state absorption.

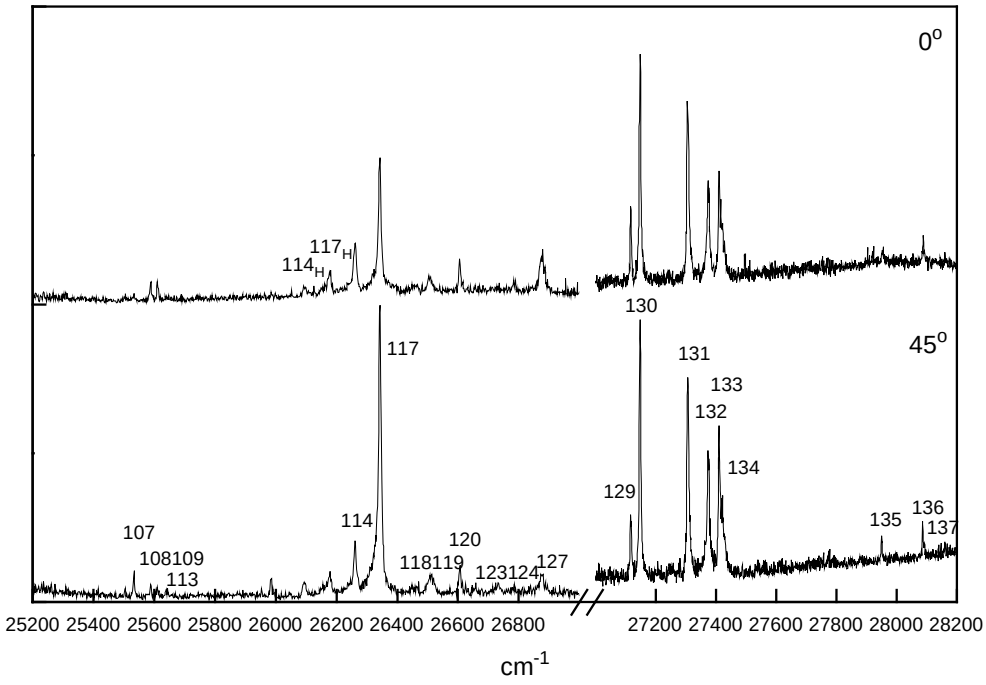

(c)

Figure 3. (Continued)

3. Results

TPE spectra from 17 800–28 200 cm^{-1} are shown in figures 3(a)–(c) with detail in figure 2. Two polarizations with $\alpha = 0$ and 45° are shown. Each peak is labelled with the sequence number of the final states assigned in table 1. Hot bands are designated with subscript H.

Assignment of the spectra, on the basis of the previously published results [1–4], including a few additional levels in a fitting at each stage, proceeds quite straightforwardly. The energy level assignments are collected in table 1. We include low energy published data for ^6H,^6F in our fitting for Cs_2NaYCl_6 :Sm [3] and also a few levels from neat $Cs_2NaSmCl_6$ from [1] near 20 000 cm^{-1}, in which spectral region we had no dye available for excitation, nor efficient Raman shifting. The observed levels are listed in sequence, and can be compared with the energies calculated using a Hamiltonian in which the crystal field is represented as a sum over one-electron operators [12]. The parameter values in wavenumbers for this Hamiltonian are given in table 2.

Where we were unable to observe sufficient levels of a manifold to confidently assign particular components $^4M_{17/2}$, $^4K_{11/2}$ and $^4L_{17/2}$, we have not included these levels in the fit, though the span of the crystal field components predicted and observed makes their assignment very probable. These levels are in parentheses in table 1.

Unidentified peaks near 21 200 cm^{-1} have been designated with an asterisk *. These lines are broader than the normal two-photon transition frequencies. We believe that absorption in this region of the spectrum must arise not only from simultaneous two-photon absorption but also from excited state absorption (ESA), because the laser is near one-photon resonance. ESA

Table 1. Energy levels of Cs_2NaYCl_6:Sm^{3+} observed and calculated (tentative assignments are in parentheses; literature values from [1] and [3]).

Level No	Term	CF level	Literature (cm^{-1})	Obs. E (cm^{-1})	Calc. E (cm^{-1})	ΔE (cm^{-1})	Multiplet deviancy
1	$^6H_{5/2}$	E_u	0	0	−2	2	0%
2	$^6H_{5/2}$	U_u	164	166	164	2	
3	$^6H_{7/2}$	E_u	1045	1046	1045	1	
4	$^6H_{7/2}$	E_u	1216	1212	1205	7	−2%
5	$^6H_{7/2}$	U_u	1210	1212	1216	−4	
6	$^6H_{9/2}$	E_u	2249		2250	−1	
7	$^6H_{9/2}$	U_u	2369		2371	−2	− < 1%
8	$^6H_{9/2}$	U_u	2423		2425	−2	
9	$^6H_{11/2}$	U_u	3654		3651	3	
10	$^6H_{11/2}$	E_u			3693		−7%
11	$^6H_{11/2}$	U_u			3703		
12	$^6H_{11/2}$	E_u	3708		3709	−1	
13	$^6H_{13/2}$	U_u			5021		
14	$^6H_{13/2}$	E_u			5025		
15	$^6H_{13/2}$	E_u			5049		
16	$^6H_{13/2}$	E_u			5144		
17	$^6H_{13/2}$	U_u			5168		
18	$^6H_{15/2}$	U_u			6295		
19	$^6F_{1/2}$	E_u	6358		6358	0	
20	$^6H_{15/2}$	U_u			6400		
21	$^6F_{3/2}$	U_u	6615		6604	11	
22	$^6H_{15/2}$	E_u			6637		
23	$^6H_{15/2}$	U_u			6764		
24	$^6H_{15/2}$	E_u			6800		
25	$^6F_{5/2}$	U_u	7107		7106	1	−11%
26	$^6F_{5/2}$	E_u	7183		7191	−8	
27	$^6F_{7/2}$	E_u			7946		
28	$^6F_{7/2}$	U_u	7955		7954	1	
29	$^6F_{7/2}$	E_u	8080		8102	−22	
30	$^6F_{9/2}$	E_u	9100		9073	27	
31	$^6F_{9/2}$	U_u	9155		9150	5	−35%
32	$^6F_{9/2}$	U_u	9180		9197	−17	
33	$^6F_{11/2}$	E_u			10 452		
34	$^6F_{11/2}$	U_u			10 487		
35	$^6F_{11/2}$	E_u			10 566		
36	$^6F_{11/2}$	U_u			10 617		
37	$^4G_{5/2}$	U_u	17 742	17 738	17 723	15	−7%
38	$^4G_{5/2}$	E_u	18 089	18 082	18 091	−9	
39	$^4F_{3/2}$	U_u	18 808	18 803	18 816	−13	
40	$^4G_{7/2}$	E_u			19 807		
41	$^4G_{7/2}$	U_u	19 972		19 953	19	
42	$^4G_{7/2}$	E_u	20 130		20 118	12	

Table 1. (Continued)

Level No	Term	CF level	Literature (cm^{-1})	Obs. E (cm^{-1})	Calc. E (cm^{-1})	ΔE (cm^{-1})	Multiplet deviancy
43	$^4M_{15/2}$	U_u			20 344		
44	$^4I_{9/2}$	U_u	20 389		20 377	12	
45	$^4M_{15/2}$	U_u			20 505		
46	$^4I_{9/2}$	E_u			20 548		
47	$^4I_{9/2}$	U_u	20 553		20 577	−24	
48	$^4M_{15/2}$	E_u			20 632		
49	$^4I_{11/2}$	E_u		20 856	20 858	−2	
50	$^4M_{15/2}$	U_u			20 955		
51	$^4I_{11/2}$	E_u		20 936	20 963	−27	+ 5%
52	$^4I_{11/2}$	U_u		21 080	21 072	8	
53	$^4I_{11/2}$	E_u		21 114	21 123	−9	
54	$^4I_{11/2}$	U_u		21 231	21 215	16	
55	$^4I_{13/2}$	E_u		(21 440)	21 436		
56	$^4I_{13/2}$	U_u		(21 465)	21 445		
57	$^4I_{13/2}$	E_u		(21 485)	21 472		−6%
58	$^4I_{13/2}$	U_u		21 515	21 506	9	
59	$^4I_{13/2}$	E_u		21 515	21 516	−1	
60	$^4F_{5/2}$	E_u	22 055	22 034	22 010	24	−34%
61	$^4F_{5/2}$	U_u	22 112	22 095	22 102	−7	
62	$^4M_{17/2}$	E_u		(22 332)	22 368		
63	$^4M_{17/2}$	E_u			22 379		−18%
64	$^4M_{17/2}$	U_u			22 378		
65	$^4M_{17/2}$	U_u		(22 350)	22 390		
66	$^4G_{9/2}$	U_u	22 514	22 514	22 530	−6	
67	$^4G_{9/2}$	E_u		22 573	22 570	3	
68	$^4I_{15/2}$	U_u		22 700	22 687	13	
69	$^4G_{9/2}$	U_u	22 766	22 728	22 754	−26	
70	$^4I_{15/2}$	U_u		22 859	22 828	31	
71	$^4M_{17/2}$	E_u			22 873		
72	$^4I_{15/2}$	U_u		(22 901)	22 882		
73	$^4I_{15/2}$	E_u		(22 901)	22 880		
74	$^4I_{15/2}$	E_u			23 086		
75	$^4I_{15/2}$	U_u		23 123	23 104	12	
76	$^6P_{5/2}$	E_u	23 660	23 659	23 676	−17	+ 93%
77	$^6P_{5/2}$	U_u	23 721	23 715	23 705	10	
78	$^4M_{19/2}$	E_u			23 835		
79	$^4M_{19/2}$	U_u			23 860		
80	$^4M_{19/2}$	E_u			23 891		
81	$^4M_{19/2}$	E_u			23 982		
82	$^4M_{19/2}$	U_u			24 009		
83	$^4M_{19/2}$	E_u			24 245		
84	$^4M_{19/2}$	U_u			24 251		
85	$^4L_{13/2}$	E_u		24 395	24 396	−1	
86	$^4L_{13/2}$	U_u		24 416	24 405	11	
87	$^4L_{13/2}$	E_u		24 462	24 481	−19	− < 1%
88	$^6P_{3/2}$	U_u		24 483	24 481	−2	

Table 1. (Continued)

Level No	Term	CF level	Literature (cm^{-1})	Obs. E (cm^{-1})	Calc. E (cm^{-1})	ΔE (cm^{-1})	Multiplet deviancy
89	$^4L_{13/2}$	U_u		24 538	24 534	4	
90	$^4L_{13/2}$	E_u		24 597	24 599	−2	
91	$^4F_{7/2}$	E_u		24 706	24 713	−7	
92	$^4F_{7/2}$	U_u		24 773	24 793	−20	
93	$^4F_{7/2}$	E_u			24 809		
94	$^4K_{11/2}$	U_u		(25 013)	25 048		
95	$^4M_{21/2}$	U_u			25 056		
96	$^4K_{11/2}$	U_u			25 082		
97	$^4M_{21/2}$	E_u			25 119		
98	$^4K_{11/2}$	E_u			25 104		
99	$^4M_{21/2}$	U_u			25 094		
100	$^4K_{11/2}$	E_u		(25 090)	25 124		
101	$^4M_{21/2}$	E_u			25 292		
102	$^4M_{21/2}$	U_u			25 306		
103	$^4L_{15/2}$	E_u			25 385		
104	$^4L_{15/2}$	U_u			25 416		
105	$^4L_{15/2}$	E_u			25 450		
106	$^4L_{15/2}$	U_u			25 517		
107	$^4G_{11/2}$	E_u		25 530	25 543	−13	
108	$^4G_{11/2}$	U_u		25 586	25 574	12	
109	$^4G_{11/2}$	E_u		25 609	25 604	5	−15%
110	$^4L_{15/2}$	U_u			25 635		
111	$^4M_{21/2}$	E_u			25 664		
112	$^4M_{21/2}$	U_u			25 668		
113	$^4G_{11/2}$	U_u		25 642	25 674	−32	
114	$^6P_{7/2}$	E_u		26 261	26 252	9	
115	$^4D_{1/2}$	E_u			26 280		
116	$^6P_{7/2}$	U_u			26 284		−16%
117	$^6P_{7/2}$	E_u		26 340	26 346	−6	
118	$^4L_{17/2}$	E_u		(26 515)	26 522		
119	$^4L_{17/2}$	U_u		(26 507)	26 536		
120	$^4L_{17/2}$	E_u		(26 604)	26 617		+ 25%
121	$^4L_{17/2}$	U_u			26 627		
122	$^4L_{17/2}$	U_u			26 644		
123	$^4L_{17/2}$	E_u		(26 732)	26 685		
124	$^4K_{13/2}$	E_u		26 781	26 776	5	
125	$^4K_{13/2}$	U_u			26 814		
126	$^4K_{13/2}$	E_u			26 849		
127	$^4K_{13/2}$	U_u		26 873	26 875	−2	
128	$^4K_{13/2}$	E_u			26 889		
129	$^4F_{9/2}$	U_u		27 116	27 106	10	
130	$^4F_{9/2}$	U_u		27 146	27 182	−36	
131	$^4D_{5/2}$	U_u		27 305	27 295	10	
132	$^4D_{5/2}$	E_u		27 373	27 365	8	
133	$^4F_{9/2}$	E_u		27 408	27 382	26	
134	$^4D_{3/2}$	U_u		27 419	27 401	−18	

Table 1. (Continued)

Level No	Term	CF level	Literature (cm^{-1})	Obs. E (cm^{-1})	Calc. E (cm^{-1})	ΔE (cm^{-1})	Multiplet deviancy
135	$^4H_{7/2}$	E_u		27 944	27 963	−19	
136	$^4H_{7/2}$	U_u		28 083	28 094	−11	+ 33%
137	$^4H_{7/2}$	E_u		28 156	28 122	34	

Table 2. Energy level parameters for Cs_2NaYCl_6:Sm^{3+}.

Parameter	$Cs_2Na\ Sm_{0.5}Y_{0.5}Cl_6$
E_{av}	47 309
F^2	79 504
F^4	59 745
F^6	40 714
α	25.4
β	−807
γ	878
ζ_{so}	1164
T^2	144
T^3	5.21
T^4	110
T^6	−265
T^7	140
T^8	326
M^0	2.49
P^2	358
$B_0^{(4)}$	2022
$B_0^{(6)}$	−354
σ	16.8
N	67

(Note $M^2 = 0.560M^0$, $M^4 = 0.310M^0$; $P^4 = 0.750P^2$, $P^6 = 0.10P^2$.)

has two possible additional frequency dependent sources. Single-photon excitation of $^6F_{11/2}$ levels near 10 600 cm^{-1} at the narrow band laser frequency can be followed by ESA of broad-band laser light (from amplified spontaneous absorption—a.s.e.), to populate states ^4I, ^4M. Alternatively a.s.e. may populate $^6F_{11/2}$ levels initially, followed secondly by narrow-band laser absorption. The first of these ESA processes probes the ground state single-photon absorption transitions; the second probes excited state ($^6F_{11/2}$) single-photon transitions. Because of the several possible sources, and the possibility that they are vibronically coupled, we have not attempted to assign these transitions. Despite their presence, it is still a fairly simple matter to assign the transitions occurring by absorption of two narrow-band laser photons. The two-photon transition (38), observed near 18 100 cm^{-1} which seems (albeit unquantifiably) intense and has some residual background structure, is very likely also to be resonantly enhanced by the presence of underlying $^6F_{9/2}$ single photon states.

The spectra have been corrected in the regions 20 700–22 200, 22 200–23 900, 23 900–25 200, 25 200–27 000 and 27 000–28 200 cm^{-1} to indicate approximate relative TPE intensities that are consistent within each segment. These dye regions are indicated by an axis break within the spectra of figures 3(a)–(c). We have not attempted to obtain accurate relative intensities across the whole spectrum.

The mechanism, selection rules and polarization dependence of two-photon absorption

have been previously described within the O_h point group, applicable to the even electron systems f^6 and f^8 [7–12] which restricts observation of excited states to those having A_{1g}, E_g or T_{2g} symmetry. In contrast, the ground state of Sm^{3+} in Cs_2NaYCl_6 has E''_u symmetry within the double group applicable to odd electron systems such as f^5, from which single-colour two-photon transitions are allowed to all E'_u, E''_u, and U'_u excited states. Unlike the cases of Tb and Eu, where hot-band and Zeeman spectroscopy serve to locate excited A_{2g} and T_{1g} states, these techniques add nothing to the spectroscopy of Sm(III). Since all states of Sm(III) have u symmetry we omit this subscript.

We consider a beam propagating along [001], and define its polarization by the angle α of the electric vector with respect to [100]. When $\alpha = 0^\circ$, $E'' \rightarrow E'$ transitions are forbidden. When $\alpha = 45^\circ$, the $E'' \rightarrow E'$ intensity is at a maximum. The intensity of $E'' \rightarrow E''$ transitions is independent of α. The angular dependence of the $E'' \rightarrow U'$ intensity, however, is not constrained by symmetry, since the transition has different sources of intensity in each polarization.

Polarization data then allow us to confidently forbid the assignment of peaks to E' symmetry, should their intensity ratio $I(0^\circ)/I(45^\circ)$ be near unity, or to forbid their assignment to E'' symmetry should this ratio be small. In general a peak can be assigned to belong either to E''/U' or to E'/U' symmetry. Thus, for example, in figure 2, we assign band 133, the intensity of which is polarization dependent, to E' symmetry and the polarization independent transition 132 to E'' symmetry.

The low energy manifolds (1–36 ^{6}H, ^{6}F) are isolated and the *SLJ* labels provide a good description. The identity of their components is unambiguous. To higher energy of the optical gap, almost all the states are heavily mixed. In general, the level mixing in samarium is much more extensive than for Tb and Eu. The optically excited state manifold under study—figure 1, spanning about 10 000 cm^{-1}, is comprised of eight quartet and one sextet *SL* state, compared to only four *SL* levels in Tb/Eu: figure 1 in [12]. In addition, first order spin–orbit coupling causes considerable free-ion mixing of ^{4}F, ^{4}G and ^{6}P, ^{4}D and ^{4}K,^{4}L in particular. (In Tb(III) and Eu(III) ^{5}D, ^{5}G and ^{5}L are unmixed to first order and ^{5}H is well separated.) The assigned labels in table 1 represent the major parentage only.

4. Discussion

4.1. Crystal field parameters

Table 3 compares the crystal field parameters, and their ratio, obtained in this work (up to ^{4}H at 28 000 cm^{-1}) with previous studies. We have also fit the sextet and quartet manifolds in isolation allowing only the F, spin–orbit coupling and B parameters to vary. (Additional credence is lent to the assignment of the states, which was unchanged for these partial fittings.) The table shows that the quartet states have fourth and sixth order one-body parameters that are *increased* by 7% ($B_0^{(4)}$) and 17% ($B_0^{(6)}$) respectively in the quartet compared to the sextet manifold. (Our $N = 67$-level fit is dominated by the quartet states, so we obtain similar parameters for the quartet and quartet-plus-sextet fits.) We may observe also that the percentage deviations of the crystal field spans, shown in the final column of table 1, in the average crystal field shows a trend that becomes increasingly positive on going to higher energy. This same expansion trend is observable in our work on terbium(III) [7–11], but contrasts with the case of europium (III) [12].

The ^{6}H and ^{6}F levels of samarium(III) have been studied in neat $Cs_2NaSmCl_6$ [1] by absorption and emission spectroscopy but assignment of only 13 levels was insufficient to obtain accurate crystal field parameters. Previous parametrization based on 25–28 levels [2, 3]

Table 3. Crystal field parameters for $Cs_2NaLnCl_6:Sm^{3+}$.

Parameter	This work	This work	This work	[5]	[4]
Compound	Cs_2NaYCl_6:Sm	Cs_2NaYCl_6:Sm	Cs_2NaYCl_6:Sm	$Cs_2NaSmCl_6$	Cs_2NaYCl_6:Sm
No of levels	67	43	24	28	25
Fitting range	0–28 200 cm^{-1}	Quartets	Sextets	0–22 100 cm^{-1}	0–22 100 cm^{-1}
$\beta_0^{(4)}$	2022	2024	1896	1828	1885
$\beta_0^{(6)}$	−354	−352	−301	−315	−291

(Note $B_0^{(4)} = 1.128B_0^4$: $B_0^{(6)} = -1.277B_0^6$ for crystal field parameters, B_0^k, quoted in [4].)

in $Cs_2NaYCl_6:Sm^{3+}$ [4] and $Cs_2NaSmCl_6$ [5], are dominated by the sextet states and give crystal field parameters, both $B_0^{(4)}$ and $B_0^{(6)}$, very similar to those we obtain by fitting the sextet states alone—table 3.

The original suggestions [15, 16] were that a large part of any correlated crystal field might well be spin dependent. Spin antiparallel electrons do not experience an attractive exchange force and consequently have more extended radial wavefunctions, leading to the expectation that the higher lying, lower spin multiplicity manifolds would have larger effective crystal fields.

This prediction of an expansion in the crystal field parameters has not always been borne out by experiment [5]. However data for several non-maximum multiplicity states are really required for SCCF analysis, and these have rarely been available for cubic systems. Our preliminary analysis for samarium f^5 indicates an expansion of the crystal field is indeed manifest, in both fourth and sixth order crystal field parameters, when applied to the sextet and quartet manifolds.

The observed fractional increases in the crystal field parameters are equal, in the SCCF model [15, 16], to $(1 - 0.5c_0)$, and allow us to estimate effective SCCF parameters [12]:

$$c_0^{(4)} = -0.14 \qquad c_0^{(6)} = -0.3.$$

An opposing contraction trend in the crystal field parameters in certain lanthanides, notably europium(III), may reflect the tendency of ions to mix charge transfer (L → M) states into particular spin configurations; this spin-polarization or covalency effect [16] is unlikely to be important in Sm(III) f^5. A full SCCF analysis for Sm, Eu, Tb(III) elpasolites will be presented shortly [17].

4.2. Rogue multiplets

We have previously commented upon some 'rogue multiplets', for which the crystal field splitting is either far too large or too small relative to that predicted by calculations that use one-electron operators. Because of the mixed parentage of the free ion states, even in the absence of the crystal field, it is hard to assign deviations of the crystal field parameters as being spin–orbit specific. Table 1, however, presents results for the span (the separation of the two well defined outermost crystal field components) of those multiplets which are experimentally well defined in samarium, together with the predicted span and the deviation of the former as a percentage of the latter. (The spread of the multiplet, which we defined in [12], is not well defined unless all the component states of the manifold are defined.) A positive deviation thus represents a crystal field that exceeds the average. Since in some cases the *SLJ* labels are a serious over-simplification, we avoid a discussion of systematic deviations between calculated and experimental splittings in states where the underlying multiplet character is poorly defined. $^4H_{7/2}$ and $^6P_{5/2}$ are the manifolds which appear to be most poorly fitted by the one-body model.

A discussion of the multiplet dependence of the effective crystal field is to be presented in due course [17].

4.3. Transition intensities

Unlike the cases of Tb(III) and Eu(III), the low lying excited state manifold of Sm(III) contains states, ^{6}P, of the same spin multiplicity as the ground state, ^{6}H. Although the spectra are not scaled over the full range, it is clear that the intensities of $^6P_{3/2,5/2,7/2}$, though among the more intense features, do not dominate the rest of the spectrum by anything approaching an order of magnitude.

In the absence of the crystal field perturbation, two photon absorption can cause a maximum change $\Delta L = \pm 2$. Transitions with $\Delta L = \pm 4(^6\mathrm{P} \leftarrow {}^6\mathrm{H})$ will require a double intervention of the spin–orbit operator (whether through mixing in the ground, the virtual intermediate or the final state). The extent of the sextet–quartet spin–orbit mixing is $\approx$3% in the free-ion wavefunctions. The spin–orbit operator required to change L by one unit is available also to effect a change of spin (for instance it mixes ^{4}G into the ^{6}H ground state). Despite the spin-allowed nature of the sextet–sextet transitions it is not clear that this will provide increased intensity to the spin-allowed orbitally forbidden two-photon excitations, relative to the spin-forbidden orbitally allowed sextet–quartet transitions. Although the sextet–sextet transitions remain orbitally forbidden in both one- and two-photon spectroscopy in zero field, introduction of the crystal field perturbation will affect the applicability of the above argument.

5. Conclusions

Two-photon absorption spectroscopy has allowed the assignment of 80 crystal-field levels for Sm(III) f^5 in a cubic site. Comparison with previous, far more limited, data sets demonstrates that significant deviations from one-electron crystal field theory are manifest in lanthanide elpasolites. Preliminary analysis provides support for a spin correlated crystal field, in which there is a small expansion of the crystal field parameters with lower spin multiplicity. This result is in keeping with the expected radial increase of the 4f wavefunction for spin antiparallel electrons.

Acknowledgments

We thank the EPSRC for financial support, and the Rutherford Appleton Laboratory for the use of a dye laser through the laser loan scheme, and M F Reid for allowing us to use his F-Shell program.

References

[1] Banerjee A K and Schwartz R W 1981 *Chem. Phys.* **58** 255
[2] Foster D R, Richardson F S and Schwartz R W 1985 *J. Chem. Phys.* **82** 618
[3] Tanner P A 1989 *Chem. Phys. Lett.* **155** 59
[4] Tanner P A, Ravi Kanth Kumar V V, Jayasankar C K and Reid M F 1994 *J. Alloys Compounds* **215** 349
[5] Reid M F and Richardson F S 1985 *J. Chem. Phys.* **83** 3831
[6] Denning R G 1991 *Eur. J. Solid State Inorg. Chem.* **28** 33
[7] Berry A J, McCaw C S, Morrison I D and Denning R G 1996 *J. Lumin.* **66/67** 272
[8] Berry A J, Denning R G and Morrison I D 1997 *Chem. Phys. Lett.* **266** 195
[9] Berry A J, Denning R G and Morrison I D1997 *J. Chem. Phys.* **106** 8967
[10] Berry A J, Morrison I D and Denning R G 1998 *Mol. Phys.* **93** 1

[11] Morrison I D, Berry A J and Denning R G 1999 *Mol. Phys.* **96** 43
[12] Thorne J R G, Jones M, McCaw C S, Murdoch K M, Denning R G and Khaidukov N M 1999 *J. Phys.: Condens. Matter* **11** 7851–66
[13] Luxbacher T, Fritzer H P, Sabry-Grant R and Flint C D 1995 *Chem. Phys. Lett.* **241** 103
[14] Knudsen G P, Voss F W, Nevald R and Amberger H 1982 *The Rare Earths in Modern Science and Technology* vol 3, ed G J McCarthy and H Silber (New York: Plenum) p 335
[15] Judd B R 1977 *Phys. Rev. Lett.* **39** 242
[16] Newman D J, Siu G G and Fung W Y P 1982 *J. Phys. C: Solid State Phys.* **15** 3113
[17] Thorne J R G, McCaw C S and Denning R G in preparation